Plasmonic enhancement of Gold Nanoparticles in a microfluidic biochip

Ana Rita Trindade Antunes
MSc in Biomedical Engineering, 68404 MEBiom

under the supervision of Professor João Pedro Conde
Department of Bioengineering, Instituto Superior Técnico, INESC-MN
Dr.João Fonseca, Biosurfit, Lisboa Portugal

March 2016

Abstract

Gold Nanoparticles (AuNPs) exhibit extraordinary properties which are quite unlike those of bulk material, since the optical properties, such as localized surface plasmon resonance (LSPR), are dependent on the displayed size and shape. This work presents the adsorption of citrate stabilized spherical gold nanoparticles of 20 nm size in a microfluidic biochip, where the LSPR acquisition was made using photodiodes and photoconductors. For particle adsorption on channel surfaces, functionalization was successfully accomplished by flowing APTES inside the channel for 10 min, on which the electrostatic interaction between the gold nanoparticless and the silane resulted in full-coloured red microfluidic channels. The immobilization of the nanoparticles was sucessful flowing uninterruptedly at 1 $\mu L/min$ for 20, 30 and 75 min, in all experiments where the surface silanization was also well accomplished. The LSPR peak of these colloidal gold nanoparticles was confirmed by UV-Vis Spectroscopy, having maximum absorbance of 0.29, at 520 nm wavelength. To detect and evaluate the LSPR peak in each microchannel using photodetectors, it was necessary to couple the photodetectors with light scattering barriers aligned below the microfluidic chip. The obtained photocurrents from both devices allowed the acquisition of current spectra, in order to measure the LSPR peak, and the photocurrent measurement over time. It was analyzed that the photocurrents measurement at 520 nm decreased from initial value measured with APTES, after 10 min of flowing the gold nanoparticles, suggesting that were successfully immobilized on the channel surfaces. The spectrum acquisitions were performed after flowing the gold nanoparticles, in order to calculate absorbances values at each wavelength. The absorbance value registered a peak at plasmonic wavelength of 520 nm, in 20 min and 30 min, successfully calculated using photodiodes and photoconductors. Towards the understanding and development of simple setup for biosensing purposes in a Lab-on-a-Chip system, these findings show the possibilites to monitor in real-time gold nanoparticle interaction with biological molecules, in a robust, low cost and easily fabricated microfluidic biochip.

Keywords: *Spherical Gold Nanoparticles, LSPR, electrostatic interaction, microfluidics, photodetectors*

Introduction

This prospective study was designed to investigate a LSPR-based sensing system, in a simple Poly(dimethylsiloxane) microfuidic device, for real-time acquisition using photodetectors. In the pages that follow, it will be argued the properties of AuNPs and its application through many fields, the microfluidic chip as tool for biosensing purposes, and the photoacquisition devices used in this work.

The nanoscale size of AuNPs (20 nm) allows a high surface to volume ratio, through which chemical and physical characteristics differ from bulk material. AuNPs possess unique properties, dependent on size and shape as key parameters related to light scattering and surface chemical activity. The synthetic method for colloidal AuNPs fabrication, through gold reduction, dates back to the work of Turkevich et al.[15] and it is being developed. Each fabrication method may yield AuNPs size range from 10 to 300 nm, and different shapes such as spherical, rods, pyramides, among others, dependent of the applications of interest. Colloidal solution of AuNPs within 20 nm size range present a distinctive red colour, due to displaying an optical feature, known as LSPR. As light interacts with AuNPs, the electron cloud around the surface can oscillate at a given frequency. For these oscillations (LSPR) to occur, the AuNPs have to be much

smaller than the incident wavelength, as assigned to as the quasi-static approximation.[5] LSPR occurs within visible frequencies and yield strong optical absorbance and scattering characteristics of AuNPs. AuNPs of 20 nm size used in the present work, when isolated and, in colloidal form, display a predominant absorption intensity, with plasmon resonance peak at 520 nm wavelength, causing the extinction of respective green wavelengths, whereas transmission of red colours arise.[5] When agglomerated, the plasmon resonance shifts for longer wavelengths and the peak itself is broadened, which the red colour is consequently absorbed. The possibilities of using AuNPs widens as biosensing platforms, in colorimetric assays using Lab-on-a-Chip (LoC) systems, since the LSPR is extremely sensitive to the surrounding medium. The conduction electrons frequency of oscillation is most dependent on the external dielectric constant thereby related to the refractive index. Thus, the resonance peak is shifted to longer wavelengths, as the surrounding refractive index increases.[16] This finds purpose in biosensing for targeted molecules, where if a target binds specifically to the AuNPs, it leads to a higher average refractive index in the neighbouring medium, causing the LSPR to red shift. The increase of absorption and scattering processes, utterly dependent upon size, is of major importance in the biosensing and enhancement on sensitivity processes. So, a significant interest in developing a highly sensitive biological and chemical sensors is based on these nanosystems.

Recently, researchers have shown an increased interest in one distinct exciting field involving the use of AuNPs in the diagnostic and treatment of cancer cells.[4][10] Current methodologies for cancer diagnosis and treatment are expensive and harmful to the patient. Hence, AuNPs provide a low cost option to target only cancerous cells, without damaging the healthy ones. Although recent studies have been developed in order to investigate the interaction between colloidal AuNPs and cells [8] [12], there is still a long road for the assessment in clinical trials. Other studies were found using AuNPs for colorimetric detection of analytes, through the change in the refractive index of the surrounding medium, caused by the adsorption of target analytes.[1][11][17]

The last two decades have seen a growing trend towards the use of Poly(dimethylsiloxane)(PDMS) in the fabrication of microfluidic biochips, as platform for biosensing purposes. Not only it presents biocompatible and chemical inertness, but is also compatible for optical detection systems, since it is optically transparent from 300 nm to IR range.[2] The use of a microfluidic biochip to a Point-of-Care (PoC) device, would involve a transduction system for biomolecular detection. As seen in previous work, the biomolecular detection system based on chemiluminescent, fluorescent and colorimetric techniques are easy implemented and well established. Hence, the integration of an optical detector in a biosensing platform using AuNPs would be ideal. The immobilization of AuNPs on the surfaces of PDMS microfluidic channels for an LSPR biosensing purposes is a demanding task, being an advanced label free real-time detection method. Up to now, far too little attention has been paid to use of real-time acquisition using the AuNPs integrated in microfluidic biochips. UV−Visible Spectroscopy is the most widespread technique for the optical properties and electronic structure of nanoparticles characterization, in which the absorption bands are related to the size and shape of these particles. Whilst characterization, synthesis and biosensing, using this technique over different setups have been widely investigated [14] [3], no previous study attempted to monitorize on LSPR real-time acquisition using an combined system of PDMS channels and photodetectors.

This paper describes the implementation of LSPR detection of immobilized AuNPs on previously modified surfaces of a microfluidic channel with (3-Aminopropyl)triethoxysilane (APTES). Here, hydrogenated Amorphous Silicon (a-Si:H) p-i-n junction photodiodes and intrisinc (a-Si:H) photoconductors were chosen as integrated transducers, coupled with light scattering barriers for low noise acquisition. Photodiodes have been used previously as platform for biodetection purposes [9] [6], where a transduction system was integrated for microfluidic PoC application. These devices are suitable in LoC systems, since the photodiodes present an easy fabrication on glass, promoting an ease integration in LoC devices, also the high quantum efficiency, low dark current and low temperature of processing are desired characteristics. As for photoconductors, the higher gain in acquisition, relative affordable fabrication also offers a facilitated alternative for integration LoC applications.

This research presents a setup that allows the integration of LSPR detection in a microfluidic assay, which sheds new light on the possibilities to monitor in real-time gold nanoparticle interaction with biological molecules, in a robust, low cost and easily fabricated microfluidic biochip using these acquisition devices.

Materials and Methods

A. Experimental Procedure:

1. Fabrication of the Microfluidic Device: The microfluidic structures were fabricated using Soft Lithography process. Two different SU-8 moulds used were from INESC-MN and developed previous to this work, were used to fabricate straight chan-

nels with different dimensions. PDMS devices were prepared using the base (Sylgard 184 silicone elastomer by Dow Corning) and a curing agent (Sylgard 184 silicone elastomer by Dow Corning) using a ratio 10:1 (w:w), respectively. After stirring both in a plastic cup, it was degassed in vacuum chamber for 1 hour and 30 min, so that air bubbles were removed. This mixture was poured on top of each SU-8 mould and put in Memmert oven, at 70 °C to be baked for 1 hour and 15 min. The PDMS structure was cut and separated from the mould, then it was necessary to punch holes in the outlet and inlet spots to allow the entrance of adapters and tubes, using a syring needle tip. The glass substrate, from Menzel-Glaser, previously washed in Alconox for 30 min, then washed with acetone, isopropyl alcohol and with water, finishing with N_2 blow-dry gun. The PDMS channels and the glass substrate were sealed through surface derivatization process, performed with UV-O treatment (UVO cleaner 144AX, Jelight Company Inc.), during 11 min (6 min to clean and 5 min to exhaust). Since, during this project, INESC-MN acquired the Plasma equipment, all the following described experiments were initialized by using this prefered sealing process. PDMS and glass surfaces were put in Plasma Cleaner (Harrick Plasma), where an Oxygen plasma would perform surface oxidation for 1 min. Then, PDMS and glass were assembled together, gently and manually pressed to seal together, depicted in Fig. 1 c), and put over a hotplate at 130 °C for 5 min.

2. Immobilization of Gold Nanoparticles in microfluidic channels: APTES was purchased from Acros Organics (Thermo Fisher Scientific), to prepare a (1%) solution prepared on Deionized water (DI-water) (99%). AuNPs colloidal solution, bearing particle average size of 20±3 nm diameter, stabilized in citrate buffer, used with initial concentration of 0.05 mg/mL (1 OD), and at ca. pH 8,0 was purchased from PlasmaChem, Germany. The syringe pump was from New Era Pump Systems, Inc. For the immobilization assay, AuNPs were adsorbed in the channel, through previous APTES silanization of the channel surfaces, as illustrated in Fig. 1 d). The APTES was flowed at a rate of Q = 0.5 $\mu L/min$ for 10 min. A study approach [13] was adopted to obtain further in-depth information on which flow rates should be applied for AuNPs immobilization. Squires, et al.,[13] presented a description of these effects, using finite-element computational tools to assist and to model the analyte target transport and interaction with a sensing area, in different sizes of microfuidic biosensors. A considerable difference between the following analysis and the work seen in Squires,*et al.* is the target area. In this work, the sensing area is ideally the bottom surface of the channel of width 200 μm that is functionalized with APTES, opposing to Squires,*et al.* where it is smaller targeted-functionalized region, compared with the channel dimensions, in the bottom surface as well. By adapting the mathematical relations and fluids theoretical concepts used by this modulation, it was possible to calculate for different rates, the total flux in the cross-section area of the channel, J_D. The estimation of the corresponding assay time, in order to obtain J_D number of AuNPs/s in the used channel surface area for a given absorbance value, is demonstrated in Table 1. Each assay time was dimensioned in order to obtain the minimum absorbance value for optical detection using photodetectors.

Table 1: Different flow rates Q assumed and derived calculations.

Q ($\mu L/min$)	J_D (AuNPs/s)	$\triangle t$(min)
0,05	$3,93 \times 10^3$	366
0,5	$8,46 \times 10^3$	170
1	$1,07 \times 10^4$	135
5	$1,82 \times 10^4$	79

An inverted Olympus Microscope was used for imaging, while immobilization of the AuNPs occurred.

3. Scanning Electron Microscope: To visualize inside a microfluidic channel, SEM was performed on RAITH 150. A microfuidic channel was subjected to lower surface oxidation, a reduced exhaust time, only 3 min against the usual 5 min, accomplished in UV-O. The channel incurred a 32 min immobilization of AuNPs assay, being the PDMS manually de-sealed from the glass at the end. The glass substrate with the remained AuNPs suffered a 30 $\mathring{A}$ deposition layer of Tantalum. The acquisitions in RAITH were performed using EHT of 10 kV and using magnifications from 30.00 kX to 146.00 kX.

4. Photodetectors Integration: A (200×200 μm^2) hydrogenated Amorphous Silicon (a-Si:H) p-i-n junction photodiodes and intrisinc (a-Si:H) photoconductors were previously microfabricated in INESC-MN. PDMS microchannels substrate were manually aligned to both photodetectors, demonstrated in Fig. 1 b) using Nikon 75519, a zoom stereo microscope. Afterwards, the substrate and the photodetectors were temporarily sealed with scotch tape after positioning for measurement on the optical setup for the AuNPs immobilization acquisitions (Fig. 1 a)).

4.1 Light Barriers microfabrication: Scattered light barriers were microfabricated in a glass substrate, the Aluminum and Titanium Tungsten were deposited in Nordiko 7000, with thickness layers of 2000 $\mathring{A}$ and 1500 $\mathring{A}$, respectively, at 1.5×10^{-3}

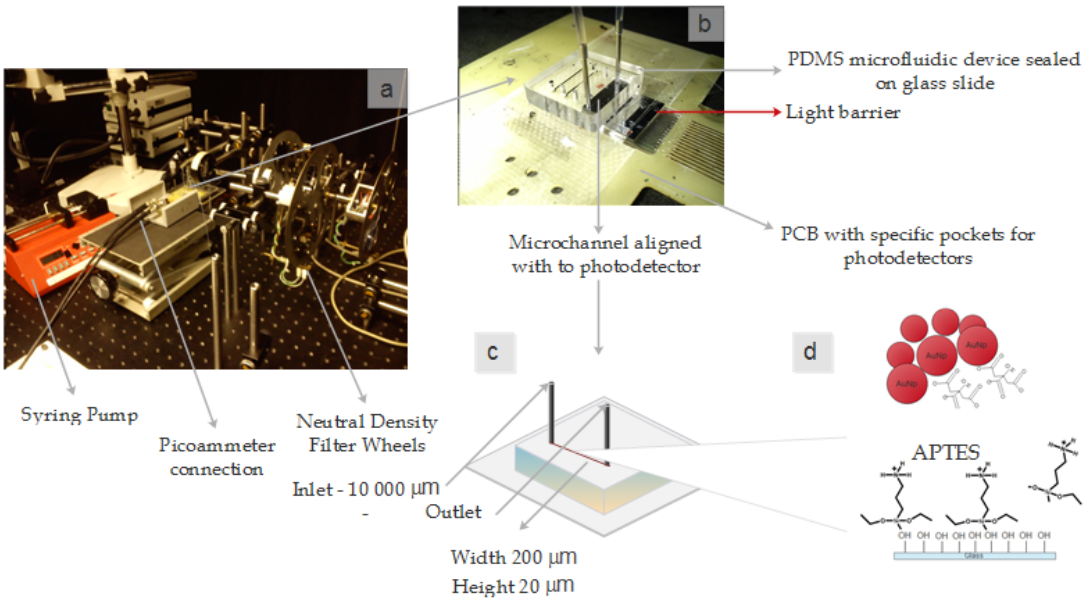

Figure 1: Photodetector integration for LSPR detection. a) Photograph of the optic apparatus for acquisition. b) Photograph of the PDMS microfluidic channels aligned to the light barrier and to the photodetector setup. c) Schematic of straight microfluidic channel used for LSPR detection. d)Illustration of the immobilization assay.

Torr, 2 kW, 3.96 V and 5.12 A. A 1,5 μm thickness DNQ-based photoresist from JSR Micro was deposited and baked for 1 min, at 90° C. This substrate was subjected to UV-laser exposure, operating at 70 keV. Next, TMA 238 WA Photoresist developer was deposited and baked for 1 min, at 106 °C. After being rinsed with acetone, water and dried with N_2 gun, the subtrate was put in the automatic dicer DAD 321 disco, which cut the subtrate into three barriers. These barriers were exposed to UV-lamp for 2 min, followed by immersed in Microstrip 30001 solution, for 20 min at 65°C, and rinsed with isopropyl alcohol. The patterning accomplished row of undeposited squares of (100×100 μm^2) to be aligned manually using Nikon 75519, on top of the photodetectors for the measurements, as seen in Fig. 1 b).

B. Data Acquisitions and Analysis:

Channel images were acquired in conditions of constant exposure of 500 μs using 20x magnification, and were treated using ImageJ (NIH) software. The central area of microchannels was imaged over time in each AuNPs immobilization experiment, where the APTES solution initially flown was taken as reference. The average of pixel intensities from these measurements facilitated the transmittance plot. The SEM acquisitions were imaged also in ImageJ (NIH) software, using FFT and 0.2% of enhanced contrast. For photodetector measurements, the photocurrents curves I-λ and I-t for each measurement were taken for the absorbance and transmittance plot, respectively. The transmittance and absorbances calculated are made possible due to the External Quantum Efficiency (EQE) of these devices, being approximately 1, which allowed that the number of electron-hole pairs detected can be considered as an intensity. The measurements were corrected using a black ink from Pelikan, Germany, flowed at the end of each experiment. This correction aimed to eliminate the contribution of the scattered light in the optic system seen in Fig. 1 a), by which the calculation of the transmittance (equation 1) and absorbance (equation 2) is demonstrated in the equations below. The I_{sample} is the photocurrent measured from the channel with AuNPs immobilization, I_0 the reference photocurrent from a channel with APTES, and I_{black} the black ink photocurrent.

$$T_{corrected} = \frac{I_{sample} - I_{black}}{I_0 - I_{black}} \quad (1)$$

$$A = -ln(T_{corrected}) \quad (2)$$

Results

In order to detect LSPR for future PoC applications in real time, measurements of immobilized AuNPs on channel surface are performed using microscopy and integrated photodetectors. With the use of two different devices it was possible to monitor AuNPs with different instrumentation, and between the two modes of acquisition (using photodiodes and photodetectors) over the signal scope. This allowed the data to be complemented by observing the signal trend over the experiment, as will be shown below.

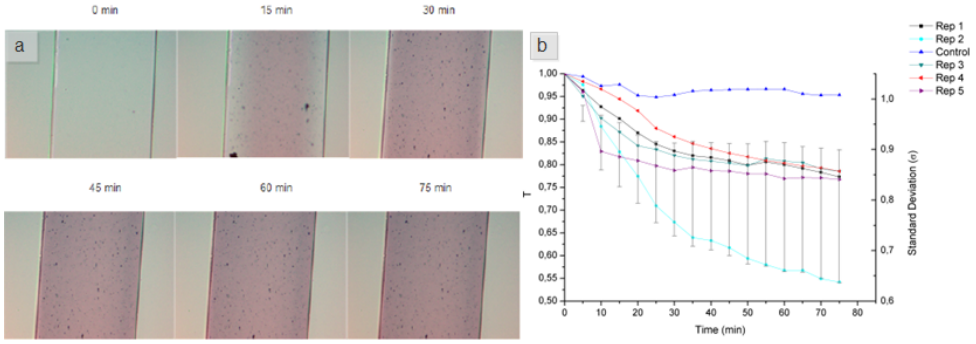

Figure 2: Immobilization experiments of AuNPs flowed at rate of 1 $\mu L/min$ during 75 min. a) Olympus microscope acquisitions in each 15 min of the micofluidic channel through immobilization time. The rose color in the channel shows the presence of adsorbed AuNPs on the surface. b) The graph shows the transmittance calculations through the measurements obtained from the microscope. This transmittance plot represents the AuNPs immobilization assay repetitions at rate of 1 $\mu L/min$ and the control experiment, where no APTES was used prior to the AuNPs. The thick line is a guide to the eye.

1.AuNPs immobilized in microfluidic channels

The strength of the electrostatic interaction between the available amine groups of the APTES and the citrate at the AuNPs surface was tested using the flow rates described in table 1, experiments showed in Fig. 2. A Q = 1 $\mu L/min$ was chosen to perform the AuNPs immobilization since it presented successful results, in terms of time spent and AuNPs used volume in each assay. Silanization of all the surfaces inside a microfuidic channel was a crucial step for the AuNPs immobilization, since without this surface functionalization the AuNPs would not be adsorbed, as shown in Fig. 2 (Control experiment), where it is plotted transmittance through time. It is shown that transmittance does not decrease due to the AuNPs, compared to other plotted experiments. Furthermore in Fig. 2 it is presented some of the experiments individually performed in channels, with chosen Q = 1$\mu L/min$ during 75 min. Although the theoretical predictions of calculated assay time, aimed for these flow rates, showed higher values (135 min) than the ones seen experimentally, the transmittance value related to an 0.02 absorbance is 0.98, accomplished within the first 10 minutes of assay. It is also shown in Fig. 2 five experiments of flowing AuNPs, where the transmittance decreases over time, reaching a usual 20% of initial value and in a specific case, decreases up to 50% of initial value. The transmittance values of these repetitions are calculated regarding the control experiment as reference, assuming a 100% in transmittance, where only APTES was flown in each channel.

2.SEM: a tool for insight

The central area of a de-sealed channel was chosen for SEM acquisitions. The acquisitions taken transversally through channel width show the aggregates of AuNPs of various sizes, distributing in different densities inside the chosen areas. Fig. 3 shows one of the acquisitions at 20 nm scale of one area in the center of the channel. The channel boudary areas acquired showed less density of AuNPs aggregates, in comparison to the center of the channel suggesting a higher concentration of these AuNPs existing in this area.

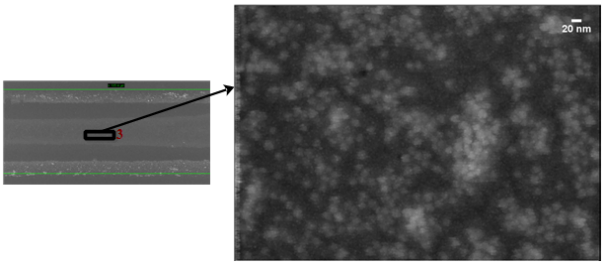

Figure 3: SEM image acquisition central area in the channel. The image was acquired with magnification of 146.00 kX.

3.LSPR detection in microfluidic channel using photodetectors

Photodiodes and photoconductors hold an area of 200×200 μm^2. Photodiodes have a typical response to absence of light of 5×10^{-14} A (dark photocurrent), whereas photoconductors have a dark photocurrent value of 7×10^{-12} A. The measurements performed in photodiodes were performed at 0 V, while in photoconductors a bias voltages of 10 and 30 V were applied. The photocurrent acquired in both detectors decreased, after the barriers were aligned on top of the photodetectors, since these barriers were opaque and possessed a row of 100×100 μm^2 squared holes ideally full aligned with the photodetector used. Also, when the PDMS microfluidic channels were placed on top and aligned, the photocurrent decreased as well, due to a decrease in the transmittance when light passed through the PDMS. Since the light barriers were developed to reduce signal noise acquisition registered in the initial experiments, there was a concern on which amount of light to be used in the experiments, to assure that the noise would not overcome the range acquisition. The Neutral Density (ND)

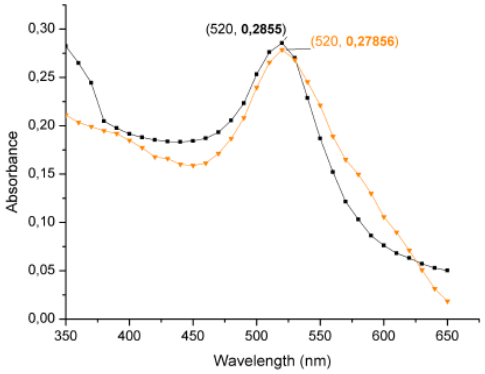

Figure 4: Comparison of absorbance values between the peak obtained by spectrophotometer (black curve) of colloidal AuNPs and the peak obtained by photodiode (orange curve), with immobilized AuNPs within the microfluidic channel after a 75 min assay.

filter wheels are a part of the optic setup, that reduce light by the rate 10^x, which a ND 3 filter reduces $10^3\times$ that reaches the sensor. In this work, the initial measurements began to be acquired with no ND filter, although an increase in dark photocurrent was registered in both devices through the long light exposure. Therefore, the following measurements were performed using ND 3 filter, and the photodetectors coupled with light barriers.

Fig. 4 shows the results of the photodiode acquisition of LSPR after 75 min of AuNPs immobilization, compared with a LSPR measurement carried out by UV-Vis Spectroscopy. The absorbance spectrum calculated for photodiodes was not corrected with black ink, and the empty channel was used as reference, not APTES, allowing a relative comparison between both methods. No ND filter and no light barrier was applied in the acquisition. The plasmon peak was obtained in a spectrophotometer from the AuNPs purchased, of 20 nm diameter size, using a circular cuvette with the original 0.05 mg/mL solution at room temperature of 24 °C. It is also shown in Fig. 4, a successful measurement of a LSPR peak visible at 520 nm wavelength, which corresponds to an absorbance value of 0.28, near the obtained value of 0.29 by spectrophotometer.

Fig. 5 shows another photodiode measurement of an interrupted AuNPs immobilization experiment. This experiment was conducted in order to evaluate if by stopping the flow rate used, an aggregation phenomena would occurr during that period. For that reason, an assay was performed in which the AuNPs were flown for 20 min, stopped for 15 min and flown again for more 30 min. The total time of the assay was about 65 min and was performed using ND 3 filter, the Al barrier and absorbance calculations used the black ink correction. In Fig.5 a) it is demonstrated the LSPR peak is at 525 nm, instead of the expected 520 nm, with an absorbance value approximately of 0.64 . The small shift in wavelength value obtained can be explained by a possible local change in medium originated by a local volume of APTES. After stopping for 15 min and flowing 30 min of AuNPs this possible local volume dispersed, since the peak was now registered at 520 nm, seen in Fig. 5 b). The higher absorbance values calculated in this experiment, can be explained by the layers formation inside the channel, that increased the interparticle interactions of AuNPs, increasing the absorbance registered at LSPR peak. Also in Fig. 5 c) it is shown the transmittance values over time of the first 20 min of flowing AuNPs, and in d) the transmittance over time of the last 30 min of flowing AuNPs inside the microfluidic channel. Instead of using the aptes spectrum raw data as reference for each wavelength, the average photocurrent measured at 520 nm, of the 10 min flowing APTES was used. The average value was then used as reference to calculate transmittance values for each time of the 20 min and 30 min of AuNPs immobilization. At 520 nm, the respective absorbance values at the end of the 20 and 30 min flowing are 0.60 and 0.81, respectively. Furthermore, the 20 min curve demonstrates that from 500 s to 800 s (8 min to 13 min) there is a $\approx$ 15 % decrease in transmittance from initial value of measured with APTES solution at the beginning of the experiment. This similar decreasing behaviour is in accordance with already seen in Fig. 2 in Olympus Microscope assays. Moreover, the final transmittance value of 20 min assay is 0.54, which is the same transmittance value that the 30 min starts with, suggesting that the 15 min between flowing did not affect the environment inside the channel. At the beginning of the assay showed in c), the transmittance suffered an abrupt variation in the 100 s of flowing, possibly due to the presence of local air bubbles that remained in the sensor area of detection, being removed by the movement of the liquid itself.

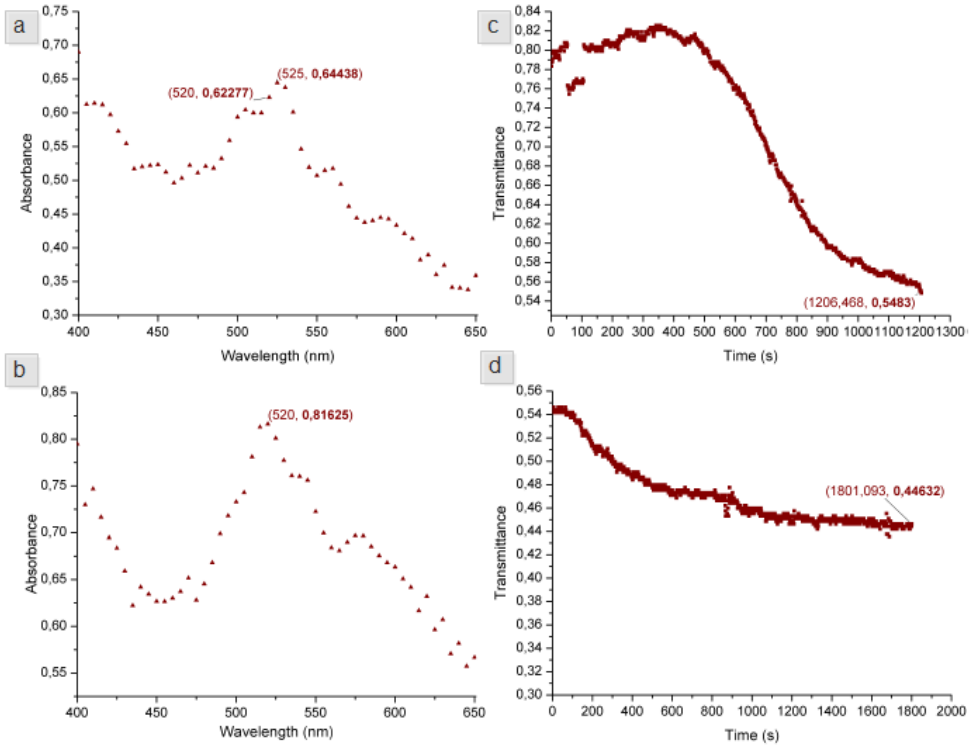

Figure 5: Photodiode acquisitions using ND3 filter and Al barrier aligned on top of the device. a) Absorbance spectrum after 20 min of AuNPs immobilization. b) Absorbance spectrum after 20+30 min of AuNPs immobilization. c) Transmittance over time of the first 20 min of flowing AuNPs. d) Transmittance over the following 30 min of flowing AuNPs.

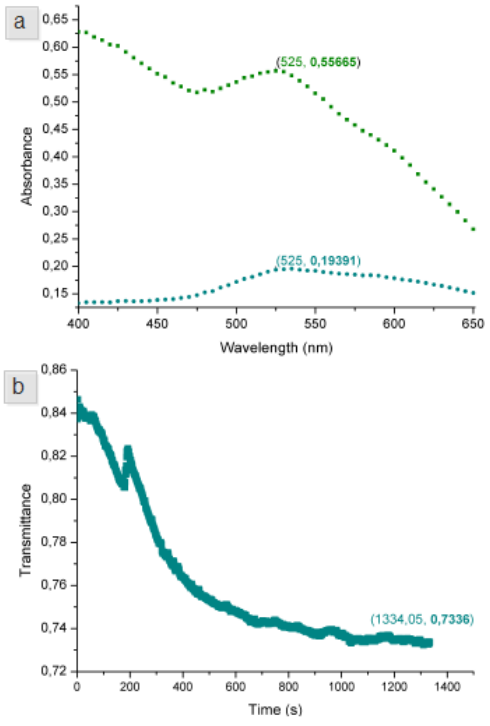

Figure 6: Photoconductor acquisition using an external applied voltage of 10 V, ND 0 filter and Al barrier. a) Absorbance spectrum of 30 min immobilization experiment (blue), compared with the yield absorbance spectrum after BSA was flowed into the same channel (green). b) Transmittance over the 30 min of flowing AuNPs into the microfluidic channel.

Fig.6 shows the photoconductor experiment, where AuNPs were flowed into a microfluidic channel for 30 min. These measurements were performed with an external voltage of 10 V, no ND filter, and the Al barrier aligned on top. The absorbance spectrum of the AuNPs immobilized after 30 min, yield a LSPR peak at 535 nm with an aproximate absorbance value of 0.20 . The shift from 520 nm to 535 nm may suggest that several layers of AuNPs were built due to a possible presence of APTES local volume, upon the photoconductor acquisition area. The shape of the absorbance spectrum differs from the expected seen in Fig. 4 from spectrophotometer, specifically those in the lower range wavelengths, due to the coincident photocurrents acquisition in the 400 nm range. After the AuNPs were adsorbed in the channel, Bovine Serum Albumine (BSA) 4% solution diluted in PBS was flowed into the channel at flow rate $Q = 0.5\ \mu L/min$ for 10 min. The yield absorbance spectrum is shown in Fig. 6 a), where it is easily identified the plasmonic peak at 525 nm wavelength with an approximate absorbance value of 0.56, higher than the absorbance value yield at 525 nm from the prior AuNPs immobilization. These higher values can be originated by the increased hindrance to light passage which originated low photocurrents acquisition, since the protein interaction and adsorption to the AuNPs occurred throughout the channel surfaces. Thus, when the photocurrent was acquired

it presented a lower value than the initial yielded from the AuNPs immobilization. Apparently, the adsorption of BSA on the AuNPs did not introduce a variation in the local refraction index, by which a shift to longer wavelengths would be seen. This interaction should be confirmed in future experiments.

The black ink correction revealed some disadvantages, since its hydrophobic behaviour yield a non-homogenous spreading in the channel. These factors arise, since it revealed some problems regarding acquisition reproducibility, which was far from being accomplished. The experiments were also subjected to several modifications, since many issues regarding scattered light as source of noise emerged in photocurrent acquisitions. Both setups used were coupled with two fabricated light barriers, in order to decrease the incoming scattered light. The inherent problems regarding the barriers were mainly about manual misalignments between the barriers and the devices, also between the barriers and the PDMS channels. In addition, the possible misaligments of the light beam and the whole setup were also considered. Throughout the assays, the acquisition system had proven to be very sensitive, embedding noise not only from light, but also from external sources, such as the introduction of liquids in the channel by the syringe pump and from the acquisition room itself.

Experiments of 75 min AuNPs immobilization were performed using ND 3 filter and the Al, performed with photoconductors, although they were not successful in accurately detecting LSPR peak, due to the noise acquired in measurements. Therefore, the TiW was microfabricated and aligned on top of the sensors to minimize signal noise acquisitions. Other 75 min AuNPs immobilization experiments were made using the new fabricated barrier, with an applied external voltage of 30 V, and ND 3 filter. None of these performed experiments was successful with the new barrier, as the acquired photocurrent showed a high degree of variation in each acquisition value, ultimately resulting in no LSPR peak detection. The photocurrent values obtained recursively revealed a scattered acquisition spectra, however in some assays there were no overlap of the spectrum acquisitions, and only the scattered values were acquired with no typical shape of the photoconductive response.

Conclusions

AuNPs have been shown promising applications for PoC devices, for its simplicity, sensitivity and speed. They also have endured optimization processes for biormarker detection limit on blood and serum samples, for early disease stages diagnosis. So far the optical characteristics and morphology of these particles have built the foundations for different signaling systems, from chemiluminescence, fuorescence to colorimetry.

These devices show differences in operation, characterization values but also in fabrication time, and associated costs, by which photodiodes are more expensive to fabricate. Current values obtained from photodiodes for dark current and black ink channel revelead much lower than the ones obtained with photoconductors. Additionally, photodiodes presented near 100% EQE, with unitary gain, while photoconductors presented lower values for EQE but higher gain values. The response time of each device was also considered in the experiments, on which photodiodes presented a response time lower than photoconductors. For lower and higher wavelengths the absorbances values are lower than expected, due to photocurrent acquisition overlapping. This may suggest that the the applied bias voltages are correlated with low EQE at these wavelengths.[7] All these factors described are influential in the decision of which type of device should be advised when detecting the plasmonic peak. Although photoconductors are relatively more affordable to fabricate, there are more promising results on photodiode experiments, since they have shown higher reproducibility and an accurate detection of the LSPR peak. This work defines the first steps towards the development of a photodetectors setup for LSPR in a microfluidic biochip. Further improvements should be considered when using these devices, in respect of scattered light exclusion method, possibly by using a suitable baseline correction (different black ink with advantageous adhesive behaviour). Also, the alignments issues should be adressed, not only for light beam but for the barriers as well. Aiming at future biological challenges not performed in this work, the optical detection of LSPR shift by photodetectors integrated in microfluidic platforms, for protein-binding is still under study. Further experiments concerning immunologic assays through colorimetric detection in photodiodes should be implemented.

Acknowledgements

The author would like to thank to Professor João Conde for all the guidance and support, as well to Dr. João Fonseca for availability shown during the brainstorming discussion at Biosurfit. Rita acknowledges also all the support from her team and coleagues at INESC-MN, which made possible this work.

References

[1] S. Gómez-De Pedro, D. Lopes, S. Miltsov, D. Izquierdo, J. Alonso-Chamarro, and M. Puyol. Optical microfluidic system based on

ionophore modified gold nanoparticles for the continuous monitoring of mercuric ion. *Sensors Actuators, B Chem.*, 194:19–26, 2014.

[2] E. Iannone. *Labs on Chip: Principles, Design and Technology*. Taylor & Francis Group, 2015.

[3] C. P. Jen, T. G. Amstislavskaya, K. F. Chen, and Y. H. Chen. Sample preconcentration utilizing nanofractures generated by junction gap breakdown assisted by self-assembled monolayer of gold nanoparticles. *PLoS One*, 10(5):1–10, 2015.

[4] A. Li Volsi, D. Jimenez de Aberasturi, M. Henriksen-Lacey, G. Giammona, M. Licciardi, and L. M. Liz-Marzán. Inulin coated plasmonic gold nanoparticles as a tumor-selective tool for cancer therapy. *J. Mater. Chem. B*, 4(6):1150–1155, 2016.

[5] O. Louis, Catherine; Pluchery. *Gold Nanoparticles for Physics, Chemistry and Biology*, volume 1. Imperial College Press, 2012.

[6] N. Madaboosi, C. R. Pedrosa, M. F. Reis, R. R. G. Soares, V. Chu, and J. P. Conde. Microfluidic ELISA for sensing of prostate cancer biomarkers using integrated a-Si : H p-i-n photodiodes *. 2:1–4, 2014.

[7] D. Misra. *Dielectrics for Nanosystems 3: Materials Science, Processing, Reliability and Manufacturing*. Electrochemical Society Transactions, 2nd edition, 2008.

[8] M. Nazarenus, Q. Zhang, M. G. Soliman, P. del Pino, B. Pelaz, S. Carregal-Romero, J. Rejman, B. Rothen-Rutishauser, M. J. D. Clift, R. Zellner, G. U. Nienhaus, J. B. Delehanty, I. L. Medintz, and W. J. Parak. In vitro interaction of colloidal nanoparticles with mammalian cells: What have we learned thus far? *Beilstein J. Nanotechnol.*, 5(1):1477–1490, 2014.

[9] P. Novo, G. Moulas, D. M. F. Prazeres, V. Chu, and J. P. Conde. Detection of ochratoxin A in wine and beer by chemiluminescence-based ELISA in microfluidics with integrated photodiodes. *Sensors Actuators, B Chem.*, 176:232–240, 2013.

[10] J. M. Seo, E. B. Kim, M. S. Hyun, B. B. Kim, and T. J. Park. Self-assembly of biogenic gold nanoparticles and their use to enhance drug delivery into cells. *Colloids Surfaces B Biointerfaces*, 135:27–34, 2015.

[11] K. Shrivas, R. Shankar, and K. Dewangan. Gold nanoparticles as a localized surface plasmon resonance based chemical sensor for on-site colorimetric detection of arsenic in water samples. *Sensors Actuators, B Chem.*, 220:1376–1383, 2015.

[12] S. J. Soenen, W. J. Parak, J. Rejman, and B. Manshian. (Intra)cellular stability of inorganic nanoparticles: Effects on cytotoxicity, particle functionality, and biomedical applications. *Chem. Rev.*, 115(5):2109–2135, 2015.

[13] T. M. Squires, R. J. Messinger, and S. R. Manalis. Making it stick: convection, reaction and diffusion in surface-based biosensors. *Nat. Biotechnol.*, 26(4):417–426, 2008.

[14] N. B. Trung, H. Yoshikawa, E. Tamiya, P. H. Viet, Y. Takamura, and T. Ashahi. Propitious immobilization of gold nanoparticles on poly(dimethylsiloxane) substrate for local surface plasmon resonance based biosensor. *Jpn. J. Appl. Phys.*, 51(3 PART 1), 2012.

[15] J. Turkevich, P. C. Stevenson, and J. Hillier. A Study of the Nucleation and Growth Processes in the Synthesis of Colloidal Gold. *Discuss. faraday Soc.*, 11(c):55–75, 1951.

[16] G. P. Wiederrecht. Handbook of Nanoscale Optics and Electronics, 2010.

[17] T. Zheng, N. Pierre-Pierre, X. Yan, Q. Huo, A. J. Almodovar, F. Valerio, I. Rivera-Ramirez, E. Griffith, D. D. Decker, S. Chen, and N. Zhu. Gold Nanoparticle-Enabled Blood Test for Early Stage Cancer Detection and Risk Assessment. *ACS Appl. Mater. Interfaces*, page 150318063129000, 2015.